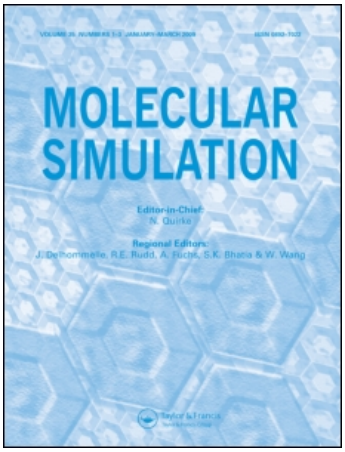

Molecular Simulation
Publication details, including instructions for authors and subscription information:
http://www.informaworld.com/smpp/title~content=t713644482

Computer Simulations of the Rheological Behavior of Confined Films

Martin Schoen[a]
[a] Institut für Theoretische Physik Technische Universität Berlin Hardenbergstr, Berlin, Germany

To cite this Article Schoen, Martin(1996) 'Computer Simulations of the Rheological Behavior of Confined Films', Molecular Simulation, 17: 4, 369 — 398
To link to this Article: DOI: 10.1080/08927029608024117
URL: http://dx.doi.org/10.1080/08927029608024117

Molecular Simulation, 1996, Vol. 17, pp. 369–398
Reprints available directly from the publisher
Photocopying permitted by license only

COMPUTER SIMULATIONS OF THE RHEOLOGICAL BEHAVIOR OF CONFINED FILMS

MARTIN SCHOEN

Institut für Theoretische Physik Technische Universität Berlin
Hardenbergstr. 36 D-10623 Berlin, Germany

(Received November 1995; accepted April 1996)

Shearing of mono- and bilayer monatomic films confined between planar solid surfaces is investigated by Monte Carlo simulations in the isostress-isostrain ensemble, where temperature, number of film atoms, relative transverse alignment of the surfaces, and applied normal stress are thermodynamic state variables. The surfaces consist of individual atoms that are identical with film atoms and are rigidly fixed in the face-centered cubic (fcc) (100) configuration. The lattice constant ℓ of the walls is varied so that the walls are either commensurate with the (solid) film at fixed nominal lattice constant ℓ_f (*i.e.* $\ell/\ell_f = 1$), homogeneously compressed ($\ell/\ell_f < 1$), or stretched ($\ell/\ell_f > 1$). Rheological properties as shear stress T_{zx} and modulus c_{44} are correlated with molecular structure of the layers, as reflected in orientational correlations. If the surfaces are properly aligned in transverse directions, then the layers exhibit a high degree of fcc order. As such ordered films are subjected to a shear strain (by reversibly moving the surfaces out of alignment), they respond initially as an elastic solid: at small strains T_{zx} depends linearly on the strain. As the shear strain increases, the response becomes highly nonlinear: T_{zx} rises to a maximum (yield point) and then decays monotonously to zero, where the maximum misalignment of the walls occurs. The dependence of T_{zx} on the shear strain up to states just beyond the yield point can be interpreted as the nonlinear response of an elastic solid to deformation. Orientational correlation functions indicate that the films are not necessarily solid, even when the walls are in proper alignment. The results suggest that the principle mechanism by which disordered nonsolid films are able to resist shearing is "pinning": the film atoms are trapped in effective cages formed by their near neighbors and mutual attraction of the walls for the caged atoms pin them together.

Keywords: Rheology; confined films; Isostress-Isostrain ensemble

I. INTRODUCTION

Recent advances in technology have made possible experimental investigations of rheological properties of confined films on the nano- or molecular

scale by means of the so-called *surface forces apparatus* (*SFA*) [1–6]. In the SFA a molecularly thin film is confined between the surfaces of two cylinders which are arranged such that their axes are at right angles. The surfaces are usually covered with mica sheets which permit a measurement of the surface separation by optical techniques [1]. Cylinder radii are macroscopic so that the surfaces may be taken to be parallel on a molecular length scale. In addition they may be perceived as planar since mica can be prepared with atomic smoothness over molecularly large areas. This setup is then immersed in a bulk reservoir of the same fluid of which the film consists. Thus, at thermodynamic equilibrium temperature T and chemical potential μ are equal in both subsystems (*i.e.* film and bulk reservoir). By exerting an external stress in the direction normal to the surfaces, the film's thickness can be altered by either expelling molecules from the film or by imbibing them from the reservoir until thermodynamic and mechanical equilibrium is established, that is until the stress exerted by the film on the surfaces equals the applied normal stress. If one measures this normal stress T_{zz} as a function of surface separation s_z, a damped oscillatory curve is obtained in many cases (see, for instance, Fig. 1 in [7]). The oscillations, which are

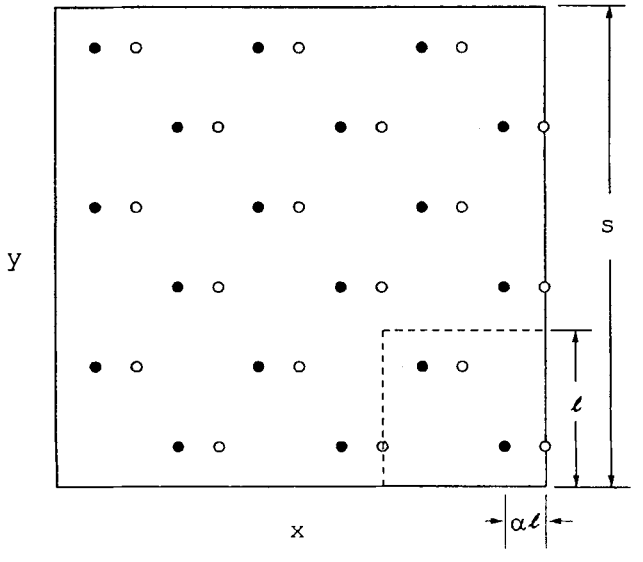

FIGURE 1 Top view of slit pore. Filled circles represent atoms in surface (1) at $z = 0$; open circles stand for atoms in wall (2) at $z = s_z$; ℓ is the lattice constant associated with the fcc (100) plane. Surfaces are depicted with shear strain (registry) $\alpha \approx 0.25$.

detected only if the molecular structure of film molecules matches the crystallographic structure of the surface to some extent, are attributed to stratification, that is the tendency of film molecules to arrange themselves in individual layers parallel with the surfaces. However, to date stratification cannot be observed directly in the SFA but has been established by computer simulations of SFA models (see [8] and references therein) and other theoretical methods such as integral equations [9–11] and density functional approaches [12, 13]. It has been demonstrated recently that stratification is accompanied by subtle order/disorder phase transitions [14, 15]. In general, stratification may be perceived as a reflection of the symmetry-breaking nature of the surfaces. Therefore, the range of the $T_{zz}(s_z)$-oscillations corresponds to the range of the film-surface interaction potential. It is then not surprising that in sufficiently thick films an inner portion exists which is homogeneous at the bulk density because μ and T are identical in both subsystems.

If, on the contrary, the films are molecularly thin comprising only, say, one or two layers of molecules the SFA permits one to expose the film to a transverse shear strain so that the conjugate shear stress can be measured as a function of the applied strain. To perform this experiment the basic setup as outlined before is modified slightly. A spring is attached to one of the surfaces and to a movable stage. The stage is moved at a constant speed, say v_x, in a direction parallel to the film's surface. The shear stress T_{zx} can then be interpreted as the (average) component of the force F_x per surface area A (pointing in z-direction) which needs to be overcome to maintain $v_x = \text{const.}$. The force F_x can be inferred from the known force constant k of the spring and its elongation x at any time during the experiment. During the course of the experiment the normal stress applied to the surfaces is held constant. Hence the conjugate strain, the surface separation (*i.e.*, the film thickness) may vary. A schematic representation of the SFA in this so-called shear mode is shown in Figure 1 of [16]. Experimentally it is found that T_{zx} increases at first and the surface connected to the spring does not move appreciably, that is the film *sticks* to the surface provided the initial relative alignment of the surfaces (*i.e.*, the registry) is favorable (see Fig. 3 in [16]). Eventually a yield stress will be reached. If the stage is moved further the movable surface *slips* across the film and the associated shear stress decays precipitously until it assumes a minimum. This stick-slip cycle repeats itself periodically provided v_x is smaller than some critical speed v_c. It is observed for all types of compounds ranging from long-chain (*e.g.* hexadecane) to spheroidal (*e.g.* OMCTS) hydrocarbons [6]. The stick-

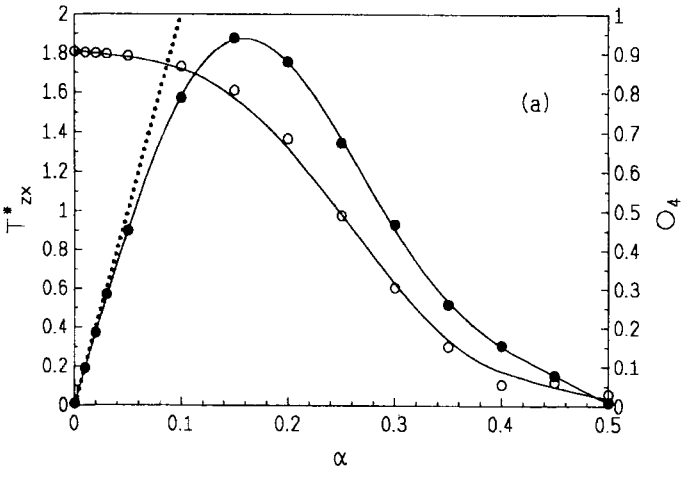

a

FIGURE 2 Shear stress T^*_{zx} (●) and mean fourfold orientational order parameter O_4 (○) *versus* registry α for monolayers. (a) $\ell/\ell_f = 16/16$; (b) $\ell/\ell_f = 15/16$; (c) $\ell/\ell_f = 16/15$. The straight dotted line (● ● ● ●) represents the limiting behavior of an elastic solid [see Eq. (23)] with $(c^0_{44})^*_{MC} = 12.6$ (a), 0.6 (c). Solid lines are intended to guide the eye.

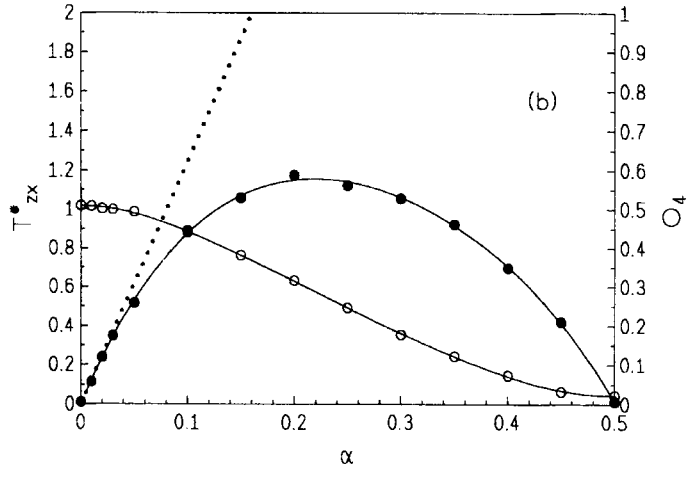

b

FIGURE 2 *Continued.*

slip cycle has been attributed by Gee *et al.* [7], to the formation of a solid-like film that pins the surfaces together (sticking regime) and must be made to flow plastically in order for the walls to slip. This suggests that the structure of the surfaces induces the formation of a solid film by means of a

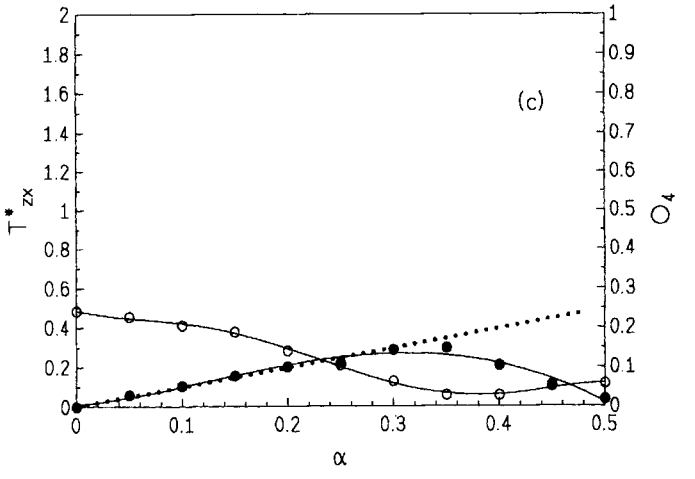

c

FIGURE 2 *Continued.*

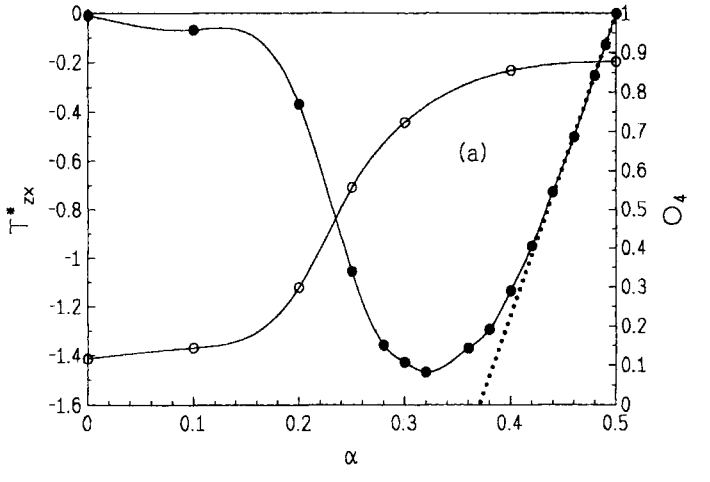

a

FIGURE 3 Same as Figure 2, except for bilayers. (a) $\ell/\ell_f = 11/11$, $(c^0_{44})^*_{MC} = 7.7$; (b) $\ell/\ell_f = 11/12$, $(c^0_{44})^*_{MC} = 2.0$.

template effect when the surfaces are properly registered and that this film "melts" when the surfaces are moved out of the correct registry. Noting that the stick-slip phenomenon is general, in that it is observed in every liquid investigated, and that the yield stress may exhibit hysteresis, Granick [6]

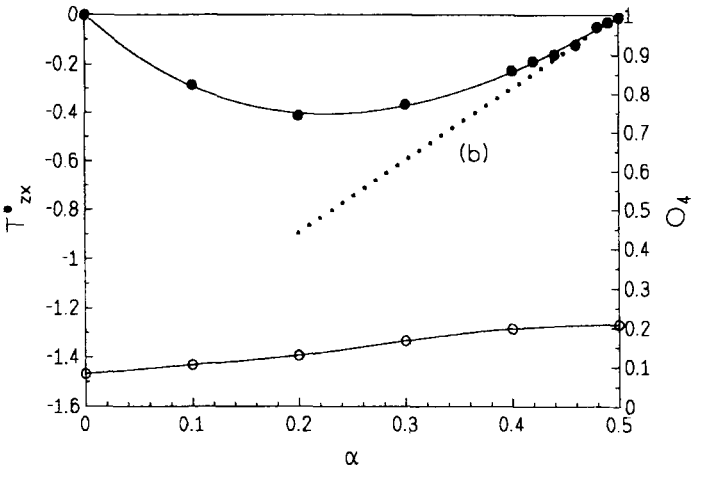

b

FIGURE 3 *Continued.*

has argued that mere confinement without involving solid-like structures may so slow mechanical relaxation of the film that flow must be activated on a time scale comparable with the experiment.

Theoretically the stick-slip phenomenon was investigated by a number of computer simulation studies based upon Monte Carlo (MC) [17–20] and nonequilibrium molecular dynamics (NEMD) [21, 22] methods in various statistical-physical ensembles which aimed at mimicking various aspects of the experimental conditions. However, all these studies employ model systems in which the surfaces induce formation of commensurate solid-like films by means of the template effect provided the surfaces are aligned favorably. In other words, the stick-slip cycle observed in computer simulations is attributed to shear strain-induced melting. However, following Granick's line of arguments [6] shear melting should be perceived as a rather special case because in most experimental systems formation of commensurate solid-like films seems highly unlikely given the extent of geometrical incompatibility between the structure of film molecules and the surfaces' crystal structure. Hence, to give a more realistic account of the experimental situation shear melting should be replaced by a more general mechanism by which thin films can still sustain a certain shear stress but do not form solid-like structures. Such a mechanism is proposed here based upon MC simulations to be presented in Sec. V. Rheological and structural properties of interest are defined in Sec, IV. In Sec. III the isostress-isostrain

ensemble is summarized in which the MC simulations are performed. However, the paper begins in Sec. II with a description of the model systems on which the simulations are based.

II. THE MODEL SYSTEMS

The model system is schematized quantitatively in Figure 1. The surfaces are taken to be square, of side length s. Each surface comprises n_s^2 unit cells of side length equal to the face-centered cubic (fcc) lattice constant ℓ. Thus, $s = n_s\,\ell$ and each surface contains $N_s = 2\,n_s^2$ rigidly fixed atoms at areal density $d_s = N_s/s^2 = 2/\ell^2$. The coordinate system is so chosen that the edges of the surfaces are parallel with the x- and y-axes (Fig. 1). The lower surface (denoted by 1 and lying in the plane $z = 0$) is fixed in this coordinate frame; the upper surface (denoted by 2 and contained in the plane $z = s_z$) can be moved transversely only in the x-direction. The coordinates of the atoms in the two surfaces are therefore related by

$$\begin{aligned} x_j^{(2)} &= x_j^{(1)} + \alpha\ell \\ y_j^{(2)} &= y_j^{(1)}, \quad j = 1,2,\ldots,N_s \\ z_j^{(2)} &= z_j^{(1)} + s_z = s_z \end{aligned} \tag{1}$$

If $\alpha = 0$, the surfaces are exactly in registry; if $\alpha = 0.5$, they are exactly out of registry. In Figure 1, they are depicted in an intermediate registry. Alternatively, one may regard α as the shear-strain parameter: $\alpha\ell z/s_z$ is the shear strain in the x-direction in planes parallel with the walls.

The film, which is confined between the surfaces and constitutes *the system*, in the thermodynamic sense, consists of N mobile atoms governed by the total configurational energy

$$U = U_{FF} + U_{FS}^{(1)} + U_{FS}^{(2)} \tag{2}$$

where each term is given by a pairwise sum of Lennard-Jones (12, 6) interatomic potentials

$$u(r) = 4\varepsilon\left[\left(\frac{\sigma}{r}\right)^{12} - \left(\frac{\sigma}{r}\right)^{6}\right] \tag{3}$$

In eq. (3) ε is the depth of the attractive well and σ is the effective diameter of the hard core. The contribution from film-film interactions is

$$U_{FF} = \frac{1}{2} \sum_{i=1}^{N} \sum_{j \neq i=1}^{N} u(r_{ij}) \tag{4}$$

and that from film-surface interactions is

$$U_{FS}^{(k)} = \sum_{i=1}^{N} \sum_{j=1}^{N_s} u(r_{ij}), \quad k = 1,2 \tag{5}$$

where $r_{ij} = |\mathbf{r}_i - \mathbf{r}_j|$ is the distance between two particles located at $\mathbf{r}_i$ and $\mathbf{r}_j$ respectively and superscript k refers to the surfaces. To prevent film atoms from escaping through the walls, a hard-sphere background potential is added to U. Periodic boundary conditions are applied in the x- and y-directions to eliminate edge effects. Thus, the system, henceforth referred to as *the prototype*, is supposed to be of infinite extent in the transverse directions.

In case the film is commensurate with the walls, $N = N_s$, the number of atoms in each surface, for the monolayer, or $N = 2N_s$ for the bilayer. To construct films incommensurate with the walls, the areal density of the film, $d_f = 2/\ell_f^2$ (where ℓ_f is the fcc lattice constant of the solid film) is fixed at the areal density of the surfaces in the commensurate case and the areal density of the surfaces, $d_s = 2/\ell^2$, is varied. To maintain periodic boundary conditions, $n_s \ell = n_f \ell_f$ is maintained. The ratio of the lattice constants, $\ell/\ell_f = n_f/n_s$, is therefore a ratio of integers.

III. MONTE CARLO SIMULATIONS IN THE ISOSTRESS-ISOSTRAIN ENSEMBLE

To employ the prototype as a sufficiently realistic model of the SFA in the shear mode, two additional experimental features need to be emphasized. First, typical speeds v_x at which the stage moves (see Sec. I) are of the order of $10^{-9} - 10^{-8}$ Å ps^{-1} [6] and therefore rather small on microscopic length and time scales characteristic of relaxation processes in the film. In other words, on length and time scales of molecular processes in the film the registry of the walls changes only negligibly. Thus, one may adopt an

idealized, quasistatic (*i.e.*, reversible) description of the SFA experiment in which the thermodynamic state of the system passes through a succession of equilibrium states distinguished from each other by different registries α. Properties of these equilibrium states may then be computed by means of MC simulations in which α (besides T and T_{zz}) is chosen as a thermodynamic state variable. Second, under certain conditions drainage seems not to occur in the SFA [23], that is during the stick-slip cycle there is no exchange of matter between the film and the bulk reservior and N instead of μ becomes a proper state variable. Thus, the complete set of variables describing the thermodynamic state of the film are temperature T, amount (number of film atoms) N, interfacial area $A = s^2$, normal stress T_{zz}, and the registry, or shear strain $\alpha\ell$. The relevant thermodynamic potential pertaining to this choice of state variables may be cast as [24]:

$$d\hat{G} = -SdT + \mu dN + \gamma d\mathrm{A} - As_z dT_{zz} + T_{zx} A d(\alpha\ell) \tag{6}$$

where S denotes entropy and γ interfacial tension (which may be expressed in terms of diagonal elements of the stress tensor $\boldsymbol{T}$) [24]. From a statistical-physical perspective $\hat{G}$ is related to the partition function Ψ of the so-called isostress-isostrain ensemble defined by the set $\{T, N, A, T_{zz}, \alpha\ell\}$ *via* [24]:

$$\hat{G} = -k_B T \ln \Psi(T, N, A, T_{zz}, \alpha\ell) \tag{7a}$$

where

$$\Psi = \sum_{\{s_z\}} \exp(\beta A s_z T_{zz}) Q(T, A, s_z, \alpha\ell)\,, \tag{7b}$$

k_B is Boltzmann's constant, $\beta = (k_B T)^{-1}$, and the canonical partition function Q is given by

$$Q = Z/(\Lambda^{3N} N!) \tag{7c}$$

In eq. (7c) the configurational integral may be written as

$$Z(T, A, s_z, \alpha\ell) = \int_{V^N} d\mathbf{r}^N \exp\left[-\beta U(\mathbf{r}^N; s_z, \alpha\ell) \right]$$

$$= \prod_{i=1}^{N} \left[\int_0^{s_Z} dz_i \int_0^{s} dy_i \int_{\alpha l z_i / s_Z}^{\alpha l z_i / s_Z + s} dx_i \exp(-\beta U) \right] \tag{8}$$

In Eq. (8) $\mathbf{r}^N$ represents the $3N$-dimensional configuration of the film and $d\mathbf{r}^N$ the corresponding volume element. The second line of Eq. (8) exhibits more fully the dependence of Z on the shear strain. The thermal de Broglie wavelength is defined by $\Lambda := h(2\pi m k_B T)^{-1/2}$, where h is Planck's constant and m is the mass of a film atom. By definition, the isostress-isostrain ensemble average of a general property $G(\mathbf{r}^N; s_z)$ is given by

$$\langle G \rangle := \sum_{\{s_z\}} \int_{V^N} d\mathbf{r}^N P(\mathbf{r}^N; s_z) G(\mathbf{r}^N; s_z) \tag{9a}$$

where the isostress-isostrain probability density

$$P(\mathbf{r}^N; s_Z) = \frac{\exp[\beta(A s_z T_{zz} - U)]}{\sum_{\{s_z\}} \int_{V^N} d\mathbf{r}^N \exp[\beta(A s_z T_{zz} - U)]} \tag{9b}$$

is also introduced. Unfortunately, $P(\mathbf{r}^N; s_z)$ cannot be obtained analytically because the prototype is far too complex and a straightforward evaluation of Eq. (9a) is precluded. However, MC simulations provide a numerical route to $\langle G \rangle$ which does neither require an *a priori* nor an *a posteriori* knowledge of $P(\mathbf{r}^N; s_z)$ [25]. To obtain $\langle G \rangle$ in isostress-isostrain MC simulations one needs to invoke the importance sampling concept, that is microstates $\{\mathbf{r}^N; s_z\}$ are generated according to their absolute probability of occurrence $P(\mathbf{r}^N; s_z)$. This permits one to rewrite Eq. (9a) as

$$\langle G \rangle := \left(\sum_{\{s_z\}}' \int_{V^N} d\mathbf{r}^N G(\mathbf{r}^N; s_z) \right)' \tag{10}$$

where the prime signifies a weighted summation and integration over a restricted hypervolume of microstates in the importance-sampling sense. By performing a correlated "random" walk in microstate space, known as Markov process, MC allows one to sample microstates with a frequency *proportional* to $P(\mathbf{r}^N; s_z)$ and (the numerical estimate) $\langle G \rangle_{MC}$ can be expected to

converge towards $\langle G \rangle$ in eq. (10) provided the sequence of microstates (*i.e.* the (numerical representation of a) Markov chain) is sufficiently long [25].

As detailed in [18], the Markov chain is realized by a sequence of two consecutive stochastic events: diffusion of film atoms; homogeneous compression or dilation of the film in the normal (z) dimension. In the diffusive step a film atom, say i, is picked sequentially and displaced randomly according to

$$\mathbf{r}_{i,n} = \mathbf{r}_{i,m} + d_r(\mathbf{1} - 2\boldsymbol{\xi}) = \mathbf{r}_{i,m} + \mathbf{d} \tag{11}$$

where subscripts m and n refer to old and new trial configuration respectively, d_r is the side length of a small cube centered on $\mathbf{r}_{i,m}$, $\boldsymbol{\xi}$ is a vector whose three components are (pseudo) random numbers distributed uniformly on the interval $[0, 1]$, and $\mathbf{1} = (1, 1, 1)$. Since s_z remains fixed during the diffusive step it follows from the theory of Markov processes and from Eq. (9b) that the displacement attempt is accepted with a probability determined by the associated change in configurational energy ΔU_{nm}. The evaluation of ΔU_{nm} is the most time consuming step. Its efficiency can, however, be enhanced substantially by employing the recently proposed Taylor-expansion scheme [26]. It is based upon realizing that for a short-range, spherically symmetric potential ΔU_{nm} can be written as a sum of three terms, namely

$$\Delta U_{nm} = \Delta U^{(1)} + \Delta U^{(2)} + \Delta U^{(3)} \tag{11}$$

corresponding to interactions between the selected atom i and any other atom j separated from i by a certain distance r_{ij}. Depending on r_{ij} three different spatial zones can be identified. the outermost tertiary zone is defined such that

$$\Delta U^{(3)} = 0 \tag{12}$$

In other words, interactions between atom i and atoms j in the tertiary zone are too weak so that the transition $\mathbf{r}_{i,m} \to \mathbf{r}_{i,n}$ contributes only negligibly to ΔU_{nm}. Interactions between atom i and another atom j located in the secondary zone are again rather weak but not negligible so that

$$\Delta U^{(2)} = U^{(2)}(\mathbf{r}_{i,n}) - U^{(2)}(\mathbf{r}_{i,m}) \cong 0 \tag{13a}$$

which permits one to write $U^{(2)}(\mathbf{r}_{i,n})$ as a Taylor series in terms of the displacement vector $\mathbf{d}$:

$$U^{(2)}(\mathbf{r}_{i,n}) = U^{(2)}(\mathbf{r}_{i,m} + \mathbf{d}) = U^{(2)}(\mathbf{r}_{i,m}) + \frac{\partial U^{(2)}}{\partial \mathbf{r}_{i,m}} \cdot \mathbf{d} + ... \tag{13b}$$

truncated after the linear term. The term $\partial U^{(2)}/\partial \mathbf{r}_{i,m}$ has a transparent physical interpretation. It represents the *total* force exerted on atom i by atoms located in the secondary zone prior to the displacement of i. For atoms located in the innermost primary zone immediately surrounding atom i, a Taylor expansion analogous to Eq. (13b) is impossible because $\Delta U^{(1)}$ is too large even for relatively small $|\mathbf{d}|$. Taking the primary zone as a sphere of radius $r_1^* = 1.8$ inscribed into a cylinder of radius $r_2^* = 2.5$ and infinite height in z-direction, the secondary zone is represented by the cylinder volume surrounding the sphere and Eq. (11) can be rewritten as

$$\Delta U_{nm} = U^{(1)}(\mathbf{r}_{i,n}) - U^{(1)}(\mathbf{r}_{i,m}) + \frac{\partial U^{(2)}}{\partial \mathbf{r}_{i,m}} \cdot \mathbf{d} \tag{14}$$

Computer-time savings of about 30% over conventional computations of ΔU_{nm} [27] are achieved because only very few atoms [$O(10)$] contribute to the primary-zone configurational energies, which need to be evaluated *before* and *after* displacing atom i, and because the secondary-zone contribution needs to be evaluated only once *prior* to the displacement of i. From a more general perspective the Taylor-expansion method rests on the smoothness of the configurational-energy hypersurface for a system in thermodynamic equilibrium which has been demonstrated extensively in [26].

After N diffusive steps, the film is subjected to compression or dilation in the z-direction, which is accomplished by changing s_z by a small amount δs_z. The magnitude δs_z is adjusted during a given run so that 60–70% of the attempts are accepted. The film is compressed (or dilated) homogeneously, that is the z-coordinates of all film and wall atoms are scaled by the ratio of wall separations *before* and *after* compression (dilation). Again the change in configurational energy needs to be computed to determine whether an attempted compression (dilation) is accepted. Since only the z-component of the interatomic separation r_{ij} is affected, it is convenient to store the

TABLE I Techinical details of Monte Carlo simulations employing the Taylor-expansion method [26]

Areal density of the film d_f^*	:	0.78272
Lattice constant ℓ^*	:	1.5985
Side length of film $s^*(\ell/\ell_f)$		23.9775 (15/16) 25.5760 (16/15, 16/16) 17.5835 (11/12) 19.1820 (11/11)
Starting configuration	:	fcc (100)
Number of equilibration steps	:	$(1.5-2.5)\times 10^5$
Number of steps between computations of cumulative averages	:	4N
Total number of MC steps	:	$(4.0-30.0)\times 10^6$
Side length of displacement cube d_r^*	:	$0.05-0.13$
Radius of primary zone sphere r_1^*	:	1.8
Thickness of secondary zone cylindrical shell $\Delta r^* = r_2^* - r_1^*$ in the x,y-plane	:	0.7
Radius of neighbor list r_N	:	$2.7\,\sigma$
Potential cutoff (pressures, energies etc.) r_c	:	$3.5\,\sigma$
Displacement of surface δs_z^*	:	$0.1-0.15$
Thickness of imaginary layer used in computation of $\rho^{(1)}(z)$, Δz^*	:	0.01
Thickness of cylindrical annulus used in computation of orientational correlation functions, $\Delta\rho_{12}^*$	:	0.02

in-plane projection ρ_{ij} and recompute the configurational energy resulting from compression (dilation) using the stored ρ_{ij} and the scaled z_{ij}.

The shear strain (registry) is initially fixed at $\alpha = 0$ for the monolayer or at $\alpha = 0.5$ for the bilayer, which are the only cases to be considered. The N film atoms are then placed between the walls in a solid-like fcc (100) configuration. The Markov chain for the beginning registry is generated and relevant ensemble averages are evaluated according to the specifications enumerated in Table I, where the entries are given in terms of the customary dimensionless (starred) units [27]. The registry α is then increased (decreased) by a small amount (0.01 to 0.05), a new Markov chain initiated from the final configuration at the previous registry, and the ensemble averages evaluated. This procedure is repeated until the entire range of α is covered. In this way, all properties are obtained as functions of α at fixed N, T, and T_{zz}. If not specifically indicated, $T^* = 1.00$ and $T_{zz}^* = 0.00$ throughout this work. Any deviation from either one of these values will be indicated explicitly in the figure captions.

IV. PROPERTIES

The property of primary rheological interest in the current context is the shear stress T_{zx}, the formal expression of which follows from Eqs. (6) and (7):

$$A\,T_{zx} = \left(\frac{\partial \hat{G}}{\partial(\alpha \ell')}\right)_{T,N,A,T_{zz}} = -(\beta\Psi)^{-1}\left(\frac{\partial \Psi}{\partial(\alpha \ell')}\right)_{T,N,A,T_{zz}}$$

$$= -(\beta \Lambda^{3N} N!\Psi)^{-1} \sum_{\{s_z\}} \exp(\beta A s_z T_{zz}) \left(\frac{\partial Z}{\partial(\alpha \ell')}\right)_{T,N,A} \tag{15}$$

Depending on how the partial derivative of Z is evaluated [24], Eq. (15) yields two alternative expressions for T_{zx}. The so-called "force" expression is given by

$$A\,T_{zx} = -F_x^{(2)} = \left\langle \frac{\partial U_{FS}^{(2)}}{\partial(\alpha \ell')} \right\rangle = -\left\langle \sum_{i=1}^{N} \sum_{j=1}^{N_s} u' x_{ij}/r_{ij} \right\rangle \tag{16a}$$

where $F_x^{(2)}$ is the mean x-component of the total force exerted by the film on the upper wall. By symmetry one also has

$$F_x^{(2)} = -F_x^{(1)} \tag{16b}$$

Alternatively the "virial" expression

$$T_{zx} = T_{zx,FF} + T_{zx,FS}$$

$$= \frac{1}{2A}\left\langle \sum_{i=1}^{N} \sum_{j \neq i=1}^{N} u' \frac{x_{ij} z_{ij}}{r_{ij} s_z} \right\rangle + \frac{1}{A}\left\langle \sum_{k=1}^{2} \sum_{i=1}^{N} \sum_{j=1}^{N_s} u' \frac{x_{ij} z_{ij}}{r_{ij} s_z} \right\rangle \tag{16c}$$

may be employed where $u'(r) := du/dr$ and $x_{ij} = x_i - x_j$, and so forth in both force and virial expressions. Eqs. (16) serve as a useful check on internal consistency of the MC simulations.

Another useful rheological measure is the shear modulus defined by

$$c_{44} := \frac{\partial T_{zx}}{\partial(\alpha\ell)} = A^{-1}\frac{\partial}{\partial(\alpha\ell)}\left\langle\frac{\partial U_{FS}^{(2)}}{\partial(\alpha\ell)}\right\rangle \tag{17}$$

where the far right hand side is due to Eq. (16a). The shear modulus is the analogue of the isothermal elastic stiffness constants used to characterize homogeneous solids [28]. For the confined film there are four strains: three compressions and one shear. The subscript 4 designates the shear strain, according to the notation of [28]. A nonzero value of the shear modulus clearly indicates a film capable of sustaining a shear stress and suggests a solid or glassy phase. From its definition it is also obvious that the shear modulus itself will turn out to be a function of the shear strain $\alpha\ell$ (see Sec. V). From Eqs. (8), (15), and (17) it can be verified that

$$c_{44} = A^{-1}\left[\beta\left(\left\langle\frac{\partial U_{FS}^{(2)}}{\partial(\alpha\ell)}\right\rangle^2 - \left\langle\left(\frac{\partial U_{FS}^{(2)}}{\partial(\alpha\ell)}\right)^2\right\rangle\right) + \left\langle\frac{\partial^2 U_{FS}^{(2)}}{\partial(\alpha\ell)^2}\right\rangle\right] \tag{18}$$

The first-order partial derivatives are given in Eq. (16a) and

$$\frac{\partial^2 U_{FS}^{(2)}}{\partial(\alpha\ell)^2} = \sum_{i=1}^{N}\sum_{j=1}^{N_s}\left[u'' x_{ij}^2/r_{ij}^2 + u'/r_{ij} - u' x_{ij}^2/r_{ij}^3\right] \tag{19}$$

An analogous expression obtains if in Eqs. (17) and (18) $U_{FS}^{(2)}$ is replaced by $U_{FS}^{(1)}$ so that one may average over both types of expressions to enhance statistical accuracy.

It is then instructive to relate the rheological quantities T_{zx} and c_{44} to the film's microscopic structure. Because of the fourfold in-plane symmetry of the fcc (100) face, insight into the transverse structure of individual layers of the film is afforded by the complex fourfold in-plane order parameter

$$\chi_4(\mathbf{r}_m) := \frac{1}{4}\sum_{n=1}^{4}\exp(4i\theta_{nm}) \tag{20}$$

associated with atom m [24, 29]. The sum on n runs over the four nearest neighbors of m that lie in the same layer; θ_{nm} is the angle between the x-axis and the projection of the vector distance $\mathbf{r}_{nm} = \mathbf{r}_n - \mathbf{r}_m$ from atom m to atom n onto the x-y plane. A rough measure of the orientational order within the

given layer i is provided by the local fourfold order

$$O_4(z_i) = \left\langle \sum_{m=1}^{N_i} \chi_4(\mathbf{r}_m) \right\rangle \Big/ \langle N_i \rangle \tag{21}$$

where N_i is the number of atoms in the layer. More detailed information is afforded by the fourfold orientational correlation function, which can be written as [24]

$$g_4(\rho_{12}) = \left\langle \sum_m \sum_{n \neq m} \chi_4^*(\mathbf{r}_m)\, \chi_4(\mathbf{r}_n) \right\rangle \Big/ \left\langle \sum_m \sum_{n \neq m} 1 \right\rangle \tag{22}$$

In Eq. (22) the sums are over all pairs of atoms (m,n) in the i-th layer, for which the atoms are separated by a distance $\rho_{12} \pm \Delta\rho_{12}/2$ in the x-y plane; the denominator is just the number of such pairs. Note that formula Eq. (22) implicitly takes the film to be homogeneous and isotropic in the transverse dimensions. In this approximation g_4 is real [24].

V. RESULTS

Employing the definitions of various quantities given in the preceding section, one may now turn to a quantitative discussion of the impact of incommensurate surface structures on the rheology of confined films. The degree of incommensurability is specified by the ratio ℓ/ℓ_f (, or n_f/n, see Sec. II). In a previous study [18] a monolayer film between fcc (100) surfaces was considered which was characterized by $\ell^* = 1.5985$ or areal density $d_s^* = 0.78272$. These numbers correspond to surface atoms fixed so that the nearest-neighbor distance is $\ell^*/2^{1/2} = 1.1303$, a little larger than the separation $r_m^* = 2^{1/6} = 1.1225$ at which the Lennard-Jones (12, 6) interatomic potential is minimum. In all cases considered in this article, the areal density of the film d_f^* is set to this value. The lattice constant of the surfaces, ℓ, is adjusted so that $\ell/\ell_f = n_f/n$ where n_f and n are integers. If $\ell/\ell_f = 1$, the surfaces are commensurate with the film; if $\ell/\ell_f < 1$, the surfaces are compressed; if $\ell/\ell_f > 1$, the surfaces are stretched. The following cases are considered: (i) monolayer ($\ell/\ell_f = 16/16$, $15/16$, $16/15$); (ii) bilayer ($\ell/\ell_f = 11/11$, $11/12$).

V.1. Shear Stress

V.1.1. Commensurate Films

Plots in Figures 2a and 3a exhibit the dependence of T_{zx} on registry in detail. For the commensurate monolayer, as α increases from 0.0, T_{zx} rises from zero to a maximum (at the yield point α_y), where the shear modulus vanishes [see Eq. (17)]. For $\alpha > \alpha_y$, T_{zx} decays monotonously to zero at $\alpha = 0.5$. For the bilayer, T_{zx} behaves similarly as α *decreases* from $\alpha = 0.5$ to $\alpha = 0.0$, except that T_{zx} is negative.

By symmetry T_{zx} is periodic in α of period 1 and must vanish at $\alpha = 0.0$ and 0.5. However, depending on how many layers make up the film, it is either stable or metastable at these special points. Commensurate films with odd numbers of solid layers are stable when the walls are in registry ($\alpha = 0.0, \pm 1.0, \pm 2.0, \ldots$) and metastable when the walls are exactly out of registry ($\alpha \pm 0.5, \pm 1.5, \ldots$); films with even numbers of solid layers are stable at $\alpha = \pm 0.5, \pm 1.5, \ldots$, and metastable at $\alpha = 0.0, \pm 1.0, \pm 2.0, \ldots$. Hence, to effect a positive displacement of the upper surface confining a monolayer at $\alpha = 0.0$, one must apply a positive force to the surface. This is true for all registries in the range $0.0 < \alpha < 0.5$. At $\alpha = 0.5$, the monolayer is metastable; a slight displacement must be opposed by a force in the opposite direction in order to keep the surface in place. That is, $T_{zx} < 0$ in the range $0.5 < \alpha < 1.0$. The bilayer, on the other hand, is stable at $\alpha = 0.5$. A negative shear stress must be applied to move the upper surface toward $\alpha = 0.0$, where the bilayer film becomes metastable.

The existence of a yield point signifies the film behaves nonlinearly. As α departs from the registry of stability ($\alpha = 0.0$ for monolayer, $\alpha = 0.5$ for bilayer) the film becomes less elastic, eventually deforming plastically. This is expected to be reflected in the film's structure as a decrease in order to be discussed below in Sec. V. 2. However, in the limit that the departure of α from the registry of stability is small, elastic behavior is observed. In this regime, the shear stress can be represented as

$$T_{zx} \cong c_{44}^0 \tilde{\alpha} \ell \tag{23}$$

where $\tilde{\alpha} = \alpha$ (monolayer), or $\alpha - 0.5$ (bilayer), and c_{44}^0 is the shear modulus of the stable solid film which is computed from the expression in Eq. (18). Thus, T_{zx} from Eq. (23) can be represented as straight-line tangents to the shear stress curves in Figures 2a and 3a in the limit $\tilde{\alpha} \to 0.0$. These plots

demonstrate the reliability of c_{44}^0, but, more significantly they also reveal substantial deviations from Hookean behavior at rather small displacements. The plastic regime begins already at $\tilde{\alpha} = 0.03$ for the monolayer and $\tilde{\alpha} < -0.06$ for the bilayer. The monolayer is stiffer than the bilayer, that is c_{44}^0 for the monolayer is much greater than c_{44}^0 for the bilayer. Note that the yield point for the monolayer is displaced ($\Delta\alpha \cong 0.15$) slightly further from the registry of stability than is the yield point for the bilayer ($\Delta\alpha \cong 0.18$, $\alpha = 0.5$), although the absolute value of the yield stress supported by the monolayer is substantially greater. This is consistent with earlier results for the shearing of multiple-layer films at fixed s_z, rather than T_{zz} [17] and can be rationalized by a similar argument: as the number of layers in the film increases, the solid-like character of the layers decreases toward the center of the film and it takes less force to break down the less ordered structure of the inner layers.

It is furthermore interesting to note that the plastic regime of the film may be interpreted as the nonlinear response of an unstrained solid phase at $\tilde{\alpha} = 0.0$ to an applied shear strain. Thus, the strain dependence of c_{44} is expressed *via* a Taylor series expansion around c_{44}^0 as

$$c_{44}(\alpha\ell) = c_{44}^0 + \frac{1}{2!}\frac{\partial^2 c_{44}}{\partial(\alpha\ell)^2}\bigg|_{\tilde{\alpha}=0}(\alpha\ell)^2 + \frac{1}{4!}\frac{\partial^4 c_{44}}{\partial(\alpha\ell)^4}\bigg|_{\tilde{\alpha}=0}(\alpha\ell)^4 + \ldots. \quad (24)$$

truncated after the third non-vanishing term. By analogy with Eq. (18) the higher-order expansion coefficients $\partial^2 c_{44}/\partial(\alpha\ell)^2$and $\partial^4 c_{44}/\partial(\alpha\ell)^4$ can be expressed *in principle* in terms of ensemble averages of higher-order partial derivatives of $U_{FS}^{(2)}$ (or $U_{FS}^{(2)}$) with respect to $\alpha\ell$. They represent the nonlinear response of a solid film to an applied shear strain. Since the expansion in Eq. (24) is done with the stable solid film as reference "point" one can easily verify that odd derivatives $\partial^{(2n+1)}c_{44}/\partial(\alpha\ell)^{(2n+1)}(n = 0, 1, 2, \ldots)$ vanish because the resulting terms involve ensemble averages of terms containing odd powers of x_{ij} (cf. Eqs. (18), (19)) which vanish on account of symmetry at $\tilde{\alpha} = 0.0$. This symmetry argument would also apply to disordered films which are assumed to be homogeneous and isotropic in transverse dimensions. However, the number of terms in the surviving even derivatives $\partial^{(2n)}c_{44}/\partial(\alpha\ell)^{(2n)}$ is large and increases rapidly with n. In addition these terms are of comparable magnitude but differ in sign so that the resulting expressions are numerically useless because of partial cancellation of terms which gives rise to a vanishing "signal-to-noise" ratio [30]. To obtain infor-

mation about the higher-order elastic coefficients in Eq. (24) despite of this difficulty $c_{44}(\tilde{\alpha}\ell)$ is expressed as a polynomial

$$c_{44}(\tilde{\alpha}\ell) = a + \frac{1}{2!}b(\tilde{\alpha}\ell)^2 + \frac{1}{4!}c(\tilde{\alpha}\ell)^4 \tag{25}$$

and the set $\{a, b, c\}$ is obtained by fitting the polynomial to MC date for c_{44} at various shear strains $\alpha\ell$. A comparison of terms in Eqs. (24) and (25) permits one to obtain numerical values for the higher-order elastic coefficients. Plots in Figures 4a and 5a show the dependence of c_{44} on $\alpha\ell$ for mono-and bilayer films and demonstrate the quality of the fit which is surprisingly good in view of the large range of $\tilde{\alpha}$ considered. That is, one would not necessarily expect a film's (nonlinear) response to a shear strain

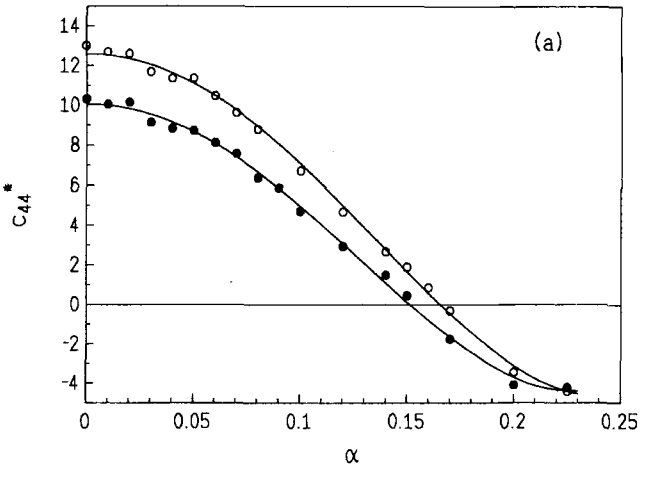

a

FIGURE 4 The shear modulus c_{44}^* *versus* shear strain $\tilde{\alpha}$ (see text) for monolayers at $T^* = 1.00$ (○), 1.25 (●) and $T_{zz}^* = -0.24$. Only commensurate cases are considered here. The solid lines represent a fit of Eq. (25) to the MC data with $(a, b, c) = (10.04, -220.68, 843.32)$ (○), $(a, b, c) = (12.593, -236.75, 812.99)$ (●) (see text). (b) The shear stress T_{zx}^* *versus* shear strain $\tilde{\alpha}$ pertaining to the thermodynamic states listed under (a). Open and closed circles represent MC data obtained from Eqs. (16), solid lines are obtained *via* Eqs. (25) and (26), and the straight dotted lines (● ● ●) represent the limiting behavior of an elastic solid [see Eq. (23)].

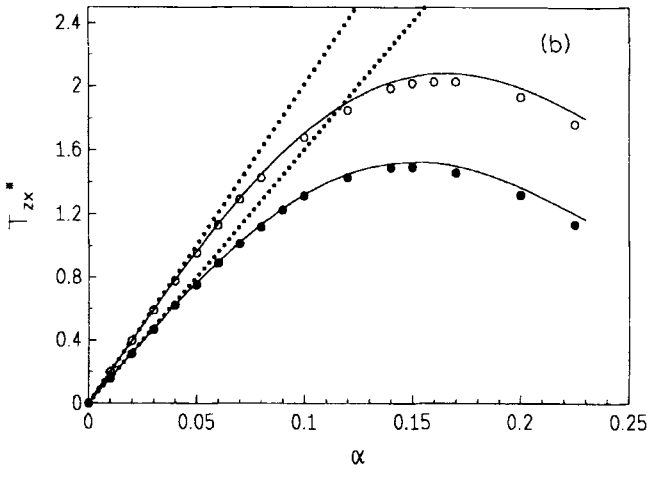

b

FIGURE 4 *Continued*

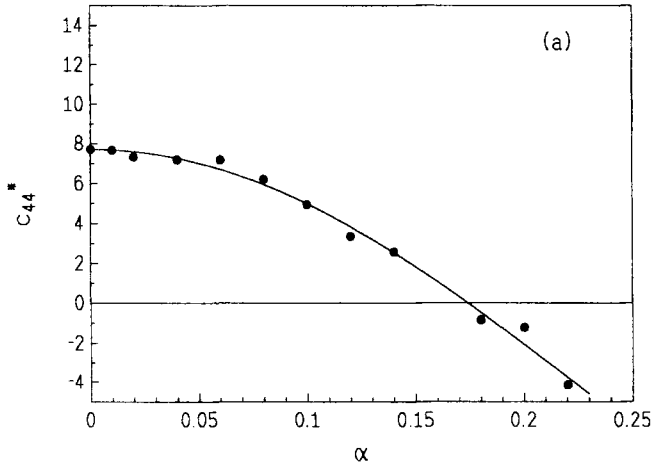

a

FIGURE 5 Same as Figure 4, except for bilayer at $T^* = 1.00$, $T^*_{zz} = -0.24$; $(a, b, c) = (7.71, -110.65, 145.35)$.

to be that of a solid-like phase over this fairly large range of strains. A further test of the fit and the internal consistency of the simulation data is provided by Eq. (17) which enables one to write

$$T_{zx}(\tilde{\alpha}\ell) = \int_0^{\tilde{\alpha}\ell} c_{44}\left[(\tilde{\alpha}\ell)'\right] d(\tilde{\alpha}\ell)' \tag{26}$$

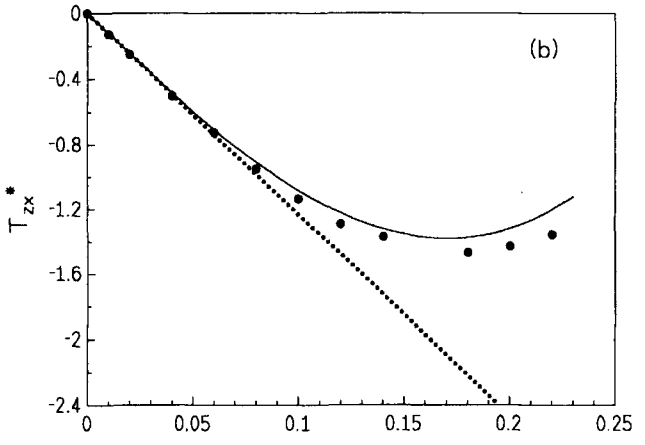

b

FIGURE 5 *Continued*

Employing Eq. (25) it is straightforward to express T_{zx} in Eq. (26) as a polynomial in terms of odd powers of $\tilde{\alpha}\ell$. The resulting curves are shown in Figures 4b and 5b together with MC data obtained directly *via* Eqs. (16). Again the agreement between the two sets of data is excellent which holds in particular for the yield point location. At larger shear strains the MC points are systematically shifted to smaller values compared with the curve obtained from Eq. (26). This can perhaps be ascribed to the neglect of higher- (sixth, eight, etc.) order terms in Eq. (24) which are expected to become increasingly important at larger $\tilde{\alpha}$. As before, the bilayer film is less stiff because its yield stress $T_{zx}(\alpha_y\ell)$ is lower than for the monolayer. This is also reflected by the values of c^0_{44} which are measures of the degree of Hookean response of the initial solid-like phase. Comparing results for the monolayer films it is concluded that confined phases become softer with increasing T in accord with one's physical intuition.

V.1.2 Incommensurate Films

Referring now to Figures 2b and 3b, it is observed that mono- and bilayer between incommensurate surfaces compressed with respect to the film exhibit the following common characteristics: the yield point is shifted

further from the registry of stability, the yield stress is lower and the film is less stiff than for the commensurate counterpart. The shifts are relatively greater for the bilayer than for the monolayer. This is perhaps not surprising, since the template effect is expected to be weaker for the more compressed surface confining the bilayer.

As can be seen in Figure 2c, stretching the walls slightly (6.66%) has a much stronger influence on the shearing behavior of the monolayer than does compressing by a comparable fraction (6.25%). The range of elasticity of the stretched-surface film appears to be extended appreciably, compared with films between commensurate or compressed surfaces.

V.2. Molecular Structural Changes Accompanying Shearing

The connection between rheological behavior of the films and their molecular structure can be seen in the dependence of the mean fourfold order parameter O_4 (see Figs. 2 and 3) and of the orientational correlation function g_4 (Figs. 6–10) on registry.

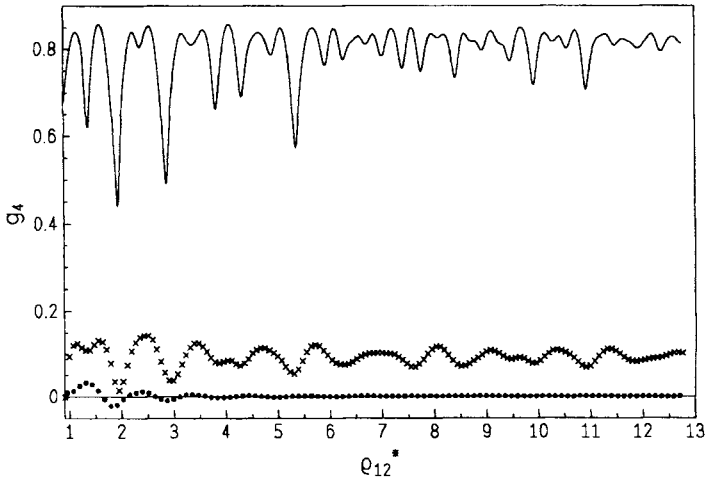

FIGURE 6 The fourfold orientational correlation function $g_4(\rho_{12})$ for monolayer as a function of intermolecular separation $\rho_{12}^*(\ell/\ell_f = 16/16)$; $\alpha = 0.0$ (—), $\alpha = 0.30$ (x x x), $\alpha = 0.50$ (● ● ●).

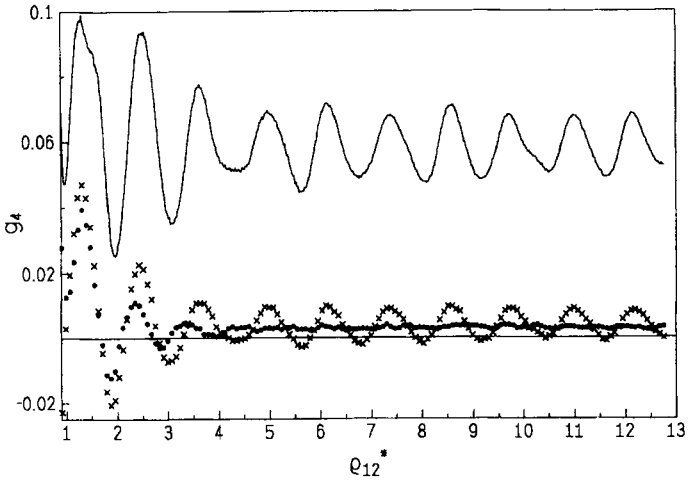

FIGURE 7 Same as Figure 6, except $\ell/\ell_f = 15/16$.

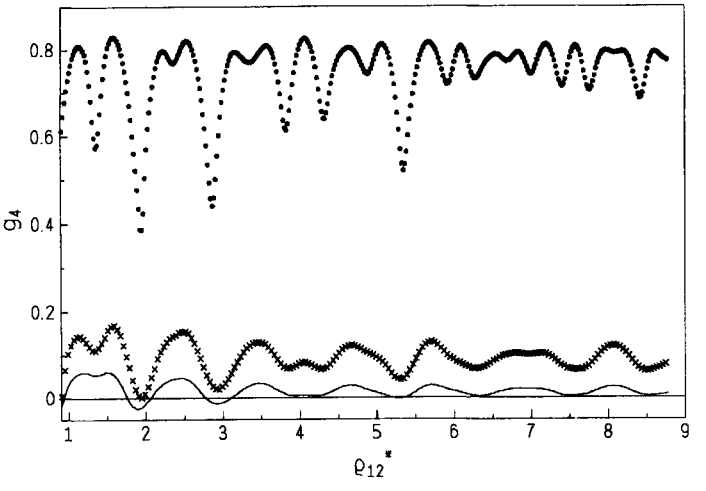

FIGURE 8 Same as Figure 6, except $\ell/\ell_f = 16/15$.

V.2.1 Commensurate Films

From Eqs. (20) and (21) $O_4 = 1.0$ is deduced for a perfect fcc (100) plane at $T^* = 0$. However, Figures 2a and 3a respectively show that $O_4 \cong 0.9$ for the

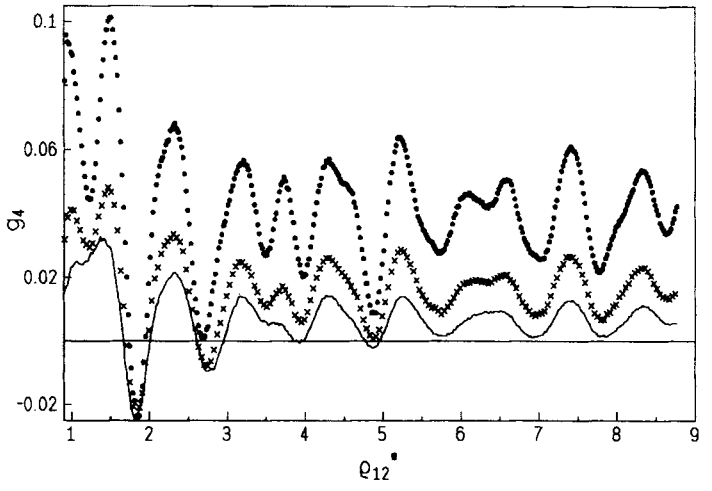

FIGURE 9 The fourfoled orientational correlation function $g_4(\rho_{12})$ for bilayer as a function of intermolecular separation $\rho_{12}^*(\ell/\ell_f = 11/11)$; $\alpha = 0.0$ (—), $\alpha = 0.20$ (x x x), and $\alpha = 0.50$ (● ● ●).

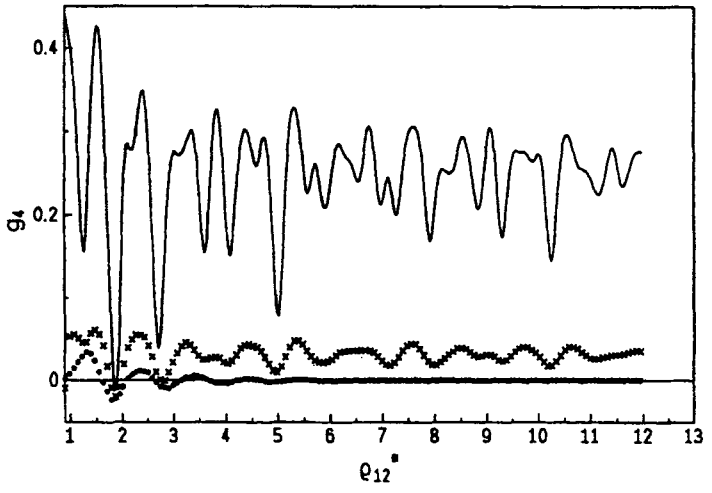

FIGURE 10 Same as Figure 9, except $\ell/\ell_f = 11/12$.

commensurate mono- and bilayers. On account of thermal motion of film molecules the film's layers are not perfectly ordered. Figures 6 and 9 also reflect the highly ordered state of the mono- and bilayer films at their respective registries of stability, $\alpha = 0.0$ and $\alpha = 0.5$. In both cases the positions

of maxima in g_4 virtually coincide with the theoretical expectation for a (thermal) fcc (100) lattice, out to $\rho_{12}^* \cong 13$ for the monolayer and $\rho_{12}^* \cong 9$ for the bilayer. At small strains, in the region of elastic behavior, O_4 remains nearly constant, reflecting the persistence of a solid-like film that responds harmonically to the applied strain. As the yield point is exceeded, O_4 declines rapidly, until the state of minimum order (*i.e.* the registry of metastability) is reached. The decrease in O_4 is mirrored in the correlation functions displayed in Figures 6 and 9, which indicate that the peaks decrease markedly in intensity and become smoother. Nevertheless, non-negligible orientational correlations clearly persist in g_4 out to the limits $\rho_{12}^* \cong 13$ (monolayer) and $\rho_{12}^* \cong 9$ (bilayer) for registries well beyond the respective yield points $\alpha_y \cong 0.3$, 0.2. It is interesting that, even at their registries of metastability, both mono- and bilayer retain a small degree of fourfold order, as seen in the nonzero values of O_4 in Figures 2a and 3a. It is particularly evident in the plot of g_4 for the bilayer (see Fig. 9). Note that for the bilayer g_4 remains long range at the registry of metastablility, whereas for the monolayer g_4 becomes short range in this limit. This can be understood because when the surfaces are completely misaligned [$\alpha = 0.5$ (monolayer), $\alpha = 0.0$ (bilayer)] the template effect of one surface can affect the structure of its contact layer (*i.e.*, the layer of film atoms closest to this surface) to a slightly larger extent if the other surface (which is misaligned with respect to the contact layer in question) is farther removed, *i.e.* if the film is thicker. Thus, the template effect is completely absent as far as the quasi two-dimensional monolayer film at $\alpha = 0.5$ is concerned because here the impact of the two competing surfaces is equal. The steady decline in O_4 with α for the monolayer (Fig. 2a) also reflects a higher (presumably second-) order phase transition, which is consistent with earlier conclusions based upon fluctuations of thermodynamic quantities [19] and on non-Brownian diffusion [20].

V.2.2 Incommensurate Films

Plots of O_4 for mono- and bilayers confined by compressed surfaces (see Figs. 2b and 3b) exhibit a dependence on registry like that of the commensurate films, except the magnitude and rate of decrease with departure of α from the registry of stability are smaller. This reflects softer films, having a lesser degree of solid-like character, as expected from the lessening of the template effect of the compressed surfaces.

The orientational correlation function for the monolayer between compressed surfaces (Fig. 7) display long-range correlations with distinctive character of a strained fcc (100) layer, although the intensity of the correlations is uniformly lower. The peaks appear to be shifted inward compared with the commensurate case (Fig. 6). For example, the peak at $\rho_{12}^* = \ell^* \cong 1.6$ in Figure. 6 lies at $\rho_{12}^* = \ell^* \cong 1.5$ in Figure 7, that is the shift in the peak's position is approximately in proportion to the shift in the lattice constant of the surface. This suggests that a compressed solid monolayer forms epitaxially on compressed surfaces in registry. As α increases, fourfold coordination declines.

In contrast to the monolayer, the bilayer between compressed surfaces is characterized by an order parameter O_4 varying only slightly around 0.2, the value of O_4 for the monolayer near $\alpha \cong 0.3$. The structures of the g_4's are also very similar. Compared with the corresponding monolayer the bilayer between compressed surfaces exhibits a lesser degree of fcc (100)-like fourfold order as reflected by the intensity of peaks in g_4 which is smaller by roughly a factor 4–6 (see Figs. 7 and 10). It should be emphasized that, although the monolayer between compressed surfaces clearly displays features of a compressed solid-like fcc (100) film, the bilayer between compressed surfaces lacks any strong fcc-like order. The surfaces are presumably too much compressed.

For the monolayer between stretched walls the fourfold order parameter O_4 at $\alpha = 0.0$ is less by a factor of about two than O_4 for the monolayer between compressed surfaces (see Fig. 2b). Scrutinizing the plots creatively, one can descry the remnants of fcc (100) structure in g_4 (Fig. 8), with peaks much reduced in magnitude and shifted to greater ρ_{12} compared with the commensurate monolayer. Note that fourfold correlations persist out to long distances ($\rho_{12}^* \cong 13$) even at the registry of metastability.

The compressed surfaces induce a compressed fcc (100) monolayer at $\alpha = 0.0$, whereas the stretched surfaces cannot sustain a monolayer having clearly identifiable fcc character. This is supported by values for the average surface separation, $\langle s_z \rangle$, which suggest that neither of the former fits as well between the surfaces as does the latter (see, for instance, Tab. III of [24]). Moreover, the stretched-surface monolayer fits less well than the compressed-surface one. The twelve near neighbors of each film atom (four in each surface and four in the film) conspire to cage the atom. If the surfaces are not too much compressed, then the near-neighbor film atoms can move closer to form a tighter, albeit less stable cage. All atoms are cooperatively caged to

make up a compressed film. On the other hand, if the walls are stretched a little too much, the resulting cages are too loose to render the film truly solid.

VI. DISCUSSION AND CONCLUSIONS

The original motivation for this work was a desire to clear up an apparent contradiction observed in earlier simulations [8, 18] of shearing of prototypal commensurate mono- and bilayer films at constant T, N, and T_{zz}. The term "shear melting" was applied to the transition leading from a solid-like film at $\tilde{\alpha} = 0.0$, displaying features in precise correspondence to those of the fcc (100) plane, to a state whose structure is very similar to fluid-like layers that are far removed from the walls in thick films [31], at least if one examines their structure only as far as the third near-neighbor shell, which was the limit imposed by the size of the simulation cell in [18]. Nevertheless, this fluid-like film is capable of sustaining a considerable shear stress. Here is the contradiction: to support a shear stress, the film would seem to possess a rigidity characteristic of a solid and therefore to exhibit the long-range order of a solid phase.

The results of the present simulations indeed show that fourfold orientational order characteristics of the fcc (100) phase persist for values of α far beyond the yield point in the monolayer films between both commensurate and compressed surfaces. In fact, for films between commensurate surfaces a surprisingly large fraction of the shear stress curve $T_{zz}(\tilde{\alpha}\ell)$ can be predicted on the basis of a model in which the film is viewed as a solid responding nonlinearly to an applied shear strain. For both, mono- and bilayer films, this model turns out to be applicable beyond the yield point.

The behavior of the monolayer between stretched surfaces is distinctly different from that of its counterpart between compressed surfaces. Although the former displays long-range fourfold orientational order, it is very much weaker. Moreover, the structure of g_4 hardly bears a resemblance to the form of g_4 for the fcc (100) plane. With imagination one may argue that g_4 for the stretched-surface case results from averaging out the fine fcc details clearly discernible in the plots for the compressed-surface counterpart. However, as demonstrated in [24], short-range sixfold order of the same magnitude as the fourfold order is present in the stretched-surface monolayer at all registries. This suggests that the state of the film is quasi two-dimensional liquid with superposed weak long-range fcc order.

To separate the effects of film-film and film-surface interactions, an "ideal-gas" film was considered in [24], in which intermolecular forces among film atoms are set to zero, so that film atoms "experience" only the background potential of the rigid surfaces. The "ideal-gas" film turns out to support a substantial shear stress and also exhibits long-range fourfold orientational order which is due to the preferential occupation of the potential holes (or cages formed midway between the walls by the eight nearest neighbors about the hole) by the independent film atoms. The "ideal-gas" findings of [24] suggest that a primary mechanism by which monolayer films support a shear stress is "pinning": the mutual attraction of the film atoms in their potential holes for each surface "pins" the surfaces. The (applied) "pinning" stress has a normal component T_{zz} and a transverse component T_{zx}. The latter vanishes when $\alpha = 0.0$ or 0.5. Between these extremes of registry, the population of ideal-gas atoms in the potential holes is distributed asymmetrically in the x-direction, giving rise to a net stress opposing the applied shear strain.

Pinning is expected to be enhanced with respect to the ideal-gas limit for commensurate films, since the forces on each atom from its neighboring film atoms assists the surfaces in keeping the atom caged. On the other hand, intermolecular interactions with the film may actually weaken pinning, if the degree of incommensurability is large enough. Film-film interactions may not permit the film atoms to fit comfortably into cages. For example, the mismatch between structures the surfaces tend to "dictate" *via* the template effect and high-symmetry structures of the film leads to a disorganized film in stretched-surface cases, which consequently supports a smaller shear stress than the film between either commensurate or compressed surfaces.

The pinning mechanism is expected to operate in any monolayer film, regardless of the structure of the surfaces. The key element is the existence of potential holes between sufficiently rigid surfaces that can be occupied by film atoms. Depending on the degree of commensurability of film and surface structures and depending on the surfaces' rigidity [32], the film will be more or less ordered. Results for the bilayer support that pinning also operates in thicker films. For example, the bilayer between compressed surfaces, for which long-range fourfold orientational order is evident, but extremely weak compared with that of its commensurate counterpart, is stiffer and stronger than the monolayer between stretched surfaces. Here pinning requires film-film interactions; with the surfaces far enough apart to accomodate a bilayer, their mutual attraction to the "ideal-gas" would be negligible. The cooperation of both film-film and film-surface interactions results in the effective

caging of film atoms. The cages are in general distorted from the fcc configuration; long-range order is accordingly reduced. Pinning may therefore explain stick-slip behavior that is universally observed in SFA dynamic shear measurements of ultrathin liquid films [6].

The impact of commensurability of film and surface structures on the rheology of confined films has recently also been investigated in isostress-isostrain MC simulations conducted by Bordarier *et al.* [33]. Instead of compressing or stretching the surfaces these authors employ films composed of atoms which differ in size from the surface atoms. In addition, film-film and film-surface interactions are made different by employing different well depths ε in the Lennard-Jones potentials governing the various interactions. Bordarier *et al.*, find that their films can also support a shear stress in the absence of solid-like film structures [33] and obtain shear stress curves $T_{zx}(\tilde{\alpha}\ell)$ strikingly similar to those presented here for the incommensurate monolayer films [34]. Thus, recent simulational work [24, 33] supports the notion that "shear melting" should be regarded only as a rather special case with respect to SFA results for the rheological properties of confined films which can better be accounted for by the more general pinning mechanism advocated in this paper.

Acknowledgements

I am grateful to the Deutsche Forschungsgemeinschaft (DFG) for a Heisenberg fellowship (Scho 525/5–1) and thank the Scientific Council of Höchstleistungsrechenzentrum (HLRZ) at Forschungszentrum Jülich for a generous allotment of computer time on the Cray Y-MP where the computations were carried out.

References

[1] Israelachvili, J. N. (1991) *Intermolecular and surface forces*, 2nd Edition (Academic Press, London).
[2] Tabor, D. and Winterton, R. H. S. (1969) "The direct measurement of normal and retarded van der Waals forces", *Proc. Roy. Soc.*, **A312**, 435.
[3] Israelachvili, J. N. and Tabor, D. (1972) "The measurement of van der Waals dispersion forces in the range 1.5 to 130 nm, *Proc. Roy. Soc.*, **A331**, 19.
[4] Israelachvili, J. N. (1991) *Intermolecular and surface forces*, chapter 13, 2nd Edition (Academic Press, London).
[5] Israelachvili, J. N. and McGuiggan, P. M. (1988) "Forces between surfaces in liquids", *Science*, **241**, 795.
[6] Granick, S. (1991) "Motions and relaxations of confined liquids", *Science*, **253**, 1374.

[7] Gee, M. L., McGuiggan, P. M., Israelachvili, J. N. and Homola, A. M. (1990) "Liquid to solidlike transitions of molecularly thin films under shear", *J. Chem. Phys.*, **93**, 1895.
[8] Schoen, M. (1993) "Computer simulations of condensed phases in complex geometries", Springer, Heidelberg.
[9] Henderson, D., Abraham, F. F. and Barker, J. A. (1976) "The Ornstein-Zernike equation for a fluid in contact with a surface", *Mol. Phys.*, **31**, 1291.
[10] Fischer, J. and Methfessel, M. "Born-Green Yvon approach to the local densities of a fluid at interfaces", *Phys. Rev.*, **A22**, 2836.
[11] Zhou, Y. and Stell, G. "Fluids inside a pore-an integral equation approach. I. General formalism and hard spheres inside spherical and slit pores", *Mol. Phys.*, **66**, 767.
[12] Peterson, B. K., Gubbins, K. E., Heffelfinger, G. S., Marconi, U. and van Swol, F. (1988) "Lennard-Jones fluids in cylindrical pores: non-local theory and computer simulations", *J. Chem. Phys.*, **88**, 6487.
[13] Kierlick, E. and Rosinberg, M. L. (1990) "Free energy density functional for the inhomogeneous hard sphere fluid: application to interfacial adsorption", *Phys. Rev.*, **A42**, 3382.
[14] Schoen, M., Diestler, D. J. and Cushman, J. H. (1994) "Stratification-induced order-disorder phase transition in molecularly thin confined films", *J. Chem. Phys.*, **101**, 6865.
[15] Schoen, M. (1996), *J. Chem. Phys.*, in press.
[16] Israelachvili, J. N., McGuiggan, P., Gee, M., Homola, A., Robbins, M. and Thompson, P. (1990) "Liquid dynamics in molecularly thin films". *J. Phys. Condens. Matter 2*, **SA89**.
[17] Schoen, M., Rhykerd Jr, C. L., Diestler, D. J. and Cushman, J. H. (1989) "Shear forces in molecularly thin films", *Science*, **245**, 1223.
[18] Schoen, M., Diestler, D. J. and Cushman, J. H. (1993) "Shear melting of confined solid monolayer films", *Phys. Rev.*, **B47**, 5603.
[19] Schoen, M., Diestler, D. J. and Cushman, J. H. (1993) "Isostress-isostrain ensemble Monte Carlo simulation of a second order phase transition in a confined monolayer fluid", *Mol. Phys.*, **78**, 1097.
[20] Schoen, M., Diestler, D. J. and Cushman, J. H. (1994) "Anomalous diffusion in confined monolayer films", *Mol. Phys.*, **81**, 475.
[21] Thompson, P. A. and Robbins, M. O. (1990) "Origin of stick-slip motion in boundary lubrication", *Science*, **250**, 792.
[22] Lupkowski, M. and van Swol, F. (1991) "Ultrathin films under shear", *J. Chem. Phys.*, **95**, 1995.
[23] Israelachvili, J. N., McGuiggan, P. M. and Homola, A. M. (1988) "Dynamic properties of molecularly thin liquid films", *Science*, **240**, 189.
[24] Schoen, M., Hess, S. and Diestler, D. J. (1995) "Rheological properties of confined thin films", *Phys. Rev.*, **E52**, 2587.
[25] Wood, W. W. (1968) in "Physics of simple liquids", ed. Temperly, H. N. V. Rowlinson, J. S. Rushbrooke, G. S. North Holland (Amsterdam).
[26] Schoen, M. (1995) "Taylor-expansion Monte Carlo simulations of classical fluids in the canonical and grand canonical ensemble", *J. comput. Phys.*, **118**, 159.
[27] Allen, M. Pm and Tildesley, D. J. (1987) "Computer simulation of liquids", Clarendon (Oxford).
[28] Callen, H. (1972) "Thermodynamics", Wiley (New York), chap. 13.
[29] Weider, T., Glaser, M. A., Hanley, H. J. M. and Clark, N. A. (1993) "Shear-induced melting of two-dimensional solids", *Phys. Rev.*, **B47**, 5622.
[30] Schoen, M. Unpublished results.
[31] Schoen, M., Diestler, D. J. and Cushman, J. H. (1987) "Fluids in micropores I. Structure of a simple classical fluid in a slit-pore", *J. Chem. Phys.*, **87**, 5464.
[32] Diestler, D. J. and Schoen, M. (1996) "Fluids in micropores. V. Effects of thermal motion in the walls of a slit-micropore", *J. Chem. Phys.*, in press.
[33] Bordarier, P. Rousseau, B. and Fuchs, A. in preparation.
[34] Bordarier, P. private communication.